Magnetic moment and lifetime measurements of Coulomb-excited states in ^{106}Cd

N. Benczer-Koller, G. J. Kumbartzki, K.-H. Speidel, D. A. Torres, S. J. Q. Robinson, Y. Y. Sharon, J. M. Allmond, P. Fallon, I. Abramovic, L. A. Bernstein, J. E. Bevins, H. L. Crawford, Z. E. Guevara, A. M. Hurst, L. Kirsch, T. A. Laplace, A. Lo, E. F. Matthews, I. Mayers, L. W. Phair, F. Ramirez, and A. Wiens

Phys. Rev. C **94**, 034303 — Published 6 September 2016

DOI: 10.1103/PhysRevC.94.034303

Magnetic moment and lifetime measurements of Coulomb-excited states in ^{106}Cd

N. Benczer-Koller,[1] G. J. Kumbartzki,[1] K.-H. Speidel,[2] D. A. Torres,[3] S. J. Q. Robinson,[4] Y. Y. Sharon,[1] J. M. Allmond,[5] P. Fallon,[6] I. Abramovic,[7] L. A. Bernstein,[6,7,8] J. E. Bevins,[7] H. L. Crawford,[6] Z. E. Guevara,[3] A. M. Hurst,[6,7] L. Kirsch,[7] T. A. Laplace,[7,8] A. Lo,[7] E. F. Matthews,[7] I. Mayers,[7] L. W. Phair,[6] F. Ramirez,[3] and A. Wiens[6]

[1]*Department of Physics and Astronomy, Rutgers University, New Brunswick, New Jersey 08903, USA**
[2]*Helmholtz-Institut für Strahlen- und Kernphysik, Universität Bonn, D-53115 Bonn, Germany*
[3]*Departamento de Física, Universidad Nacional de Colombia, Carrera 30 No 45-03, Bogotá D.C., Colombia*
[4]*Physics Department, Millsaps College, Jackson, Mississippi 39210, USA*
[5]*Physics Division, Oak Ridge National Laboratory, Oak Ridge, Tennessee 37831, USA*
[6]*Nuclear Science Division, Lawrence Berkeley National Laboratory, Berkeley, California 94720, USA*
[7]*Department of Nuclear Engineering, University of California, Berkeley, CA 94720, USA*
[8]*Lawrence Livermore National Laboratory, Livermore, California 94551, USA*

Backround The Cd isotopes are well studied, but experimental data for the rare isotopes are sparse. At energies above the Coulomb barrier higher states become accessible.

Purpose Remeasure and supplement existing lifetimes and magnetic moments of low-lying states in ^{106}Cd.

Methods In an inverse kinematics reaction a ^{106}Cd beam impinging on a ^{12}C target was used to Coulomb excite the projectiles. The high recoil velocities provide a unique opportunity to measure g factors with the transient field technique and to determine lifetimes from lineshapes using the Doppler-shift attenuation method. Large-scale shell-model calculations were carried out for ^{106}Cd.

Results The g factors of the 2_1^+ and 4_1^+ states in ^{106}Cd were measured to be $g(2_1^+) = +0.398(22)$ and $g(4_1^+) = +0.23(5)$. A lineshape analysis yielded lifetimes in disagreement with published values. The new results are $\tau(^{106}\mathrm{Cd};2_1^+) = 7.0(3)$ ps and $\tau(^{106}\mathrm{Cd};4_1^+) = 2.5(2)$ ps. The meanlife $\tau(^{106}\mathrm{Cd};2_2^+) = 0.28(2)$ ps was determined from the fully Doppler-shifted γ line. Meanlives of $\tau(^{106}\mathrm{Cd};4_3^+) = 1.1(1)$ ps and $\tau(^{106}\mathrm{Cd};3_1^-) = 0.16(1)$ ps were determined for the first time.

Conclusions The newly measured $g(4_1^+)$ of ^{106}Cd is found to be only 59% of the $g(2_1^+)$. This difference can not be explained by either shell model or collective model calculations.

PACS numbers: 21.10.Ky, 25.70.De, 25.70.Hi, 27.60.+j

I. INTRODUCTION

The Cd isotopes with $Z = 48$ are very close to the magic proton $Z = 50$ shell closure. The two proton holes configuration is expected to contribute significantly to the nuclear wave functions. This aspect differentiates the Cd isotopes from the neighboring Sn isotopes, where the stability of the $Z = 50$ core restricts the nuclear structure to the valence neutrons. Indeed, the heavier Cd isotopes exhibit collective properties and the ^{112,114,116}Cd isotopes have long been examples of spherical vibrational nuclei.

However, experiments on Cd isotopes carried out by Garrett [1, 2], Ekström [3] and Stuchbery [4], among others, suggest a more complex nuclear structure for some Cd nuclei, including the existence of deformation with consequent rotational motion.

In both the light Sn and Cd isotopes the $B(E2; 2_1^+ \rightarrow 0_1^+)$ values show an increase over the values calculated in the shell model [3]. These discrepancies can be attributed to a variety of causes ranging from the possible non-equivalence of $B(E2)$'s determined either from Coulomb excitation or from lifetime measurements, or to actual structure differences caused by the two valence proton holes.

The recent measurements of lifetimes in ^{110}Sn [5] did not exhibit this enhancement of the $B(E2)$'s. Furthermore, the measured g factors in ^{110}Sn were found to be in good agreement with excitations of neutrons and a stable $Z = 50$ core.

The data presented in this paper stem from that particular experiment on ^{110}Sn. The radioactive ^{110}Sn nucleus was produced by the capture of an α particle by the nuclei in a ^{106}Cd beam impinging on a ^{12}C target. Simultaneously the beam ions were Coulomb excited by the target C nuclei, allowing the measurements of lifetimes and g factors of several states in ^{106}Cd.

The details of the experiment and analysis are extensively discussed in Ref. [5]. Only the analysis results leading to the new information about ^{106}Cd are described in the present paper. Shell-model calculations were carried out in a framework similar to that presented in Ref. [5].

The main interest of the present work was to obtain more detailed information about the nuclear structure of ^{106}Cd by searching for single-particle aspects in the nuclear properties of ^{106}Cd.

It should be noted that in many previous studies the 2_1^+ states of several Cd isotopes have been discussed within the framework of collective models with little attention paid to the single-particle structure (see e.g. [6]).

*Electronic address: nkoller@physics.rutgers.edu

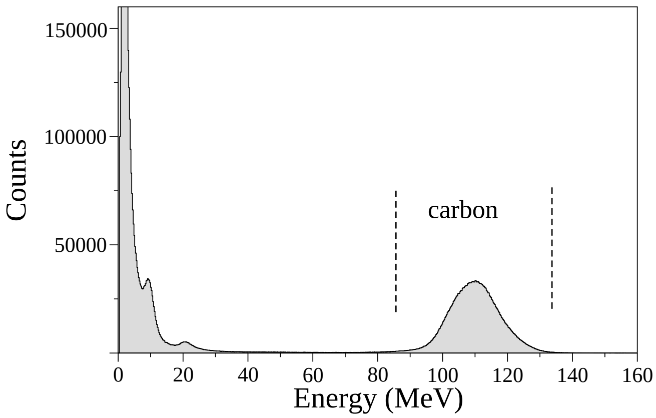

FIG. 1: Singles particle spectrum. At the beam energy of 410 MeV light particles dominate. The carbon peak is a result of Coulomb scattering of the beam projectiles in the carbon layer of the target.

II. THE EXPERIMENT

The experiment was performed at the Lawrence Berkeley National Laboratory (LBNL) 88-Inch cyclotron.

The experiment was primarily designed to measure g factors of low-lying states in ^{110}Sn via an α-particle transfer to the ^{106}Cd beam nuclei [5]. In this experiment additional data on ^{106}Cd have been obtained.

The multilayer target, front to back, consisted of 0.636 C, 8.34 Gd, 1.10 Ta, and 5.40 Cu (mg/cm^2). The beam energy was 410 MeV, close to the Coulomb barrier of ^{106}Cd on ^{12}C (390 MeV). The Coulomb excitation of the beam particles in the first target layer is established by measuring γ rays in coincidence with forward-scattered carbon ions.

The target was mounted between the pole tips of a liquid nitrogen-cooled magnet. The gadolinium layer of the target was magnetized by a field of 0.07 T. Its direction was reversed every 150 s during the measurements. The particle detector was a 300 mm^2 Si surface-barrier detector (Canberra PIPS) placed 25 mm downstream of the target at 0° to the beam direction. The beam was stopped in a 5.6 mg/cm^2 thick copper foil, placed in front of the particle detector. Only the carbon ions and light particles resulting from reactions reached the detector. The carbon particles were well separated in the 300 μm thick detector, as is shown in Fig. 1.

The γ rays were observed in four clover HPGe detectors from the ORNL and LBNL inventories. These were located 125 mm away from the target at angles of $\theta = \pm 60°$ and $\pm 120°$ with respect to the beam direction. At that distance the individual elements of the clover detectors subtended angles of $\pm 8°$ with respect to the center of the clover enclosure.

The preamplifier output signals of all detectors were digitized using a PIXIE-4 system [8]. Their time stamps and energies were written to disk. The data handling and analysis were performed as described in greater detail in

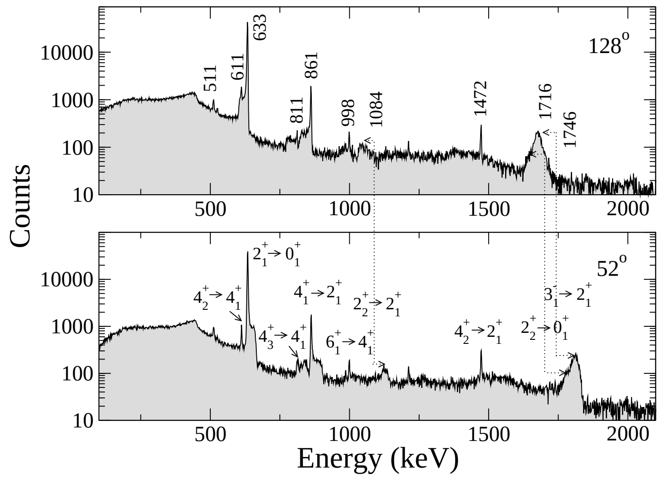

FIG. 2: Coincidence γ spectra gated on the carbon peak in Fig. 1. The spectra show the Doppler-broadened and shifted lines including the distinct lineshapes observed in a backward- and in a forward-positioned detector segment at the indicated angle θ with respect to the beam direction.

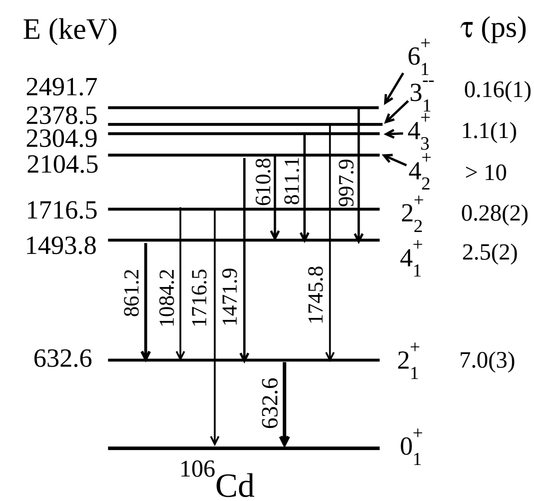

FIG. 3: Partial level scheme indicating the states in ^{106}Cd that were excited in this experiment. The energies are taken from NNDC [7]. The lifetime column shows the newly determined meanlives.

Ref. [9].

Particle-γ coincidence spectra gated on the ^{12}C peak, obtained at a beam energy of 410 MeV, are shown in Fig. 2.

The low-lying levels of ^{106}Cd that were identified in this experiment are shown in Fig. 3.

A. Precession measurement

The g factor of the 2_1^+ state in ^{106}Cd was measured previously by the transient field technique (TF) [6]. Its value was used as a check on the experiment and also served to calibrate the transient field strength.

TABLE I: The kinematic information related to the transient field measurement at a beam energy of 410 MeV. $< E >_{\rm in}$, $< E >_{\rm out}$, $< v/v_0 >_{\rm in}$ and $< v/v_0 >_{\rm out}$ are the average energies, in MeV, and velocities, in units of $v_0 = e^2/\hbar$, the Bohr velocity, of the excited probe ions as they enter into, and exit from, the gadolinium layer. $T_{\rm eff}$ is the effective time the transient field acts on the ions traversing the ferromagnetic layer.

Nucleus	$< E >_{\rm in}$	$< E >_{\rm out}$	$< v/v_0 >_{\rm in}$	$< v/v_0 >_{\rm out}$	$T_{\rm eff}$ (fs)
^{106}Cd	232	46	9.4	4.2	715

In a TF measurement the spin precession of the aligned nuclei traversing the magnetized ferromagnetic layer causes a rotation of the angular distribution of the decay γ radiation. The precession angle is derived from counting-rate changes in the stationary γ detectors when the polarizing magnetic field at the target, which is perpendicular to the detection plane of the γ detectors, is reversed. The so-called rate effect ϵ, as described in many publications (e.g. [10]), is calculated from peak intensities in the spectra of four γ detectors. Together with the logarithmic slope, $\mathrm{S}(\theta_\gamma) = (1/\mathrm{W}(\theta_\gamma))\cdot \mathrm{d}W/\mathrm{d}\theta_\gamma$ of the angular correlation relevant for the precession, the precession angle

$$\Delta\theta = \frac{\epsilon}{\mathrm{S}(\theta_\gamma)} = g \cdot \frac{\mu_{\rm N}}{\hbar} \cdot \int_{t_{\rm in}}^{t_{\rm out}} B_{\rm TF}(v(t),\, Z) \cdot e^{-t/\tau}\mathrm{d}t$$

is obtained. In the above expression g is the g factor of the excited state and μ_N is the nuclear magneton. $B_{\rm TF}$ is the effective transient field acting on the nucleus during the time interval $(t_{\rm out} - t_{\rm in})$ spent by the ions in the gadolinium layer. The exponential factor accounts for the nuclear decay during the transit time of the ions through the gadolinium layer. The relevant kinematic information for the transient-field calculation is summarized in Table I.

The angular correlations for the states were also derived from the precession data. The peak intensities of the $2_1^+ \to 0_1^+$ and $4_1^+ \to 2_1^+$ transitions in the spectra of each clover crystal, summed over both field directions and corrected for relative efficiencies, were fitted to the angular-correlation function

$$W(\theta_\gamma) = 1 + A_2 \cdot Q_2 \cdot P_2(\cos\theta_\gamma) + A_4 \cdot Q_4 \cdot P_4(\cos\theta_\gamma).$$

Here the $P_k(\cos\theta_\gamma)$ are the Legendre polynomials, the A_k are the experimental angular-correlation coefficients, which depend on the multipolarity of the γ-ray transition, and the Q_k are attenuation coefficients accounting for the finite solid angle of the γ detectors. Representative fits are shown in Fig. 3 of Ref. [5].

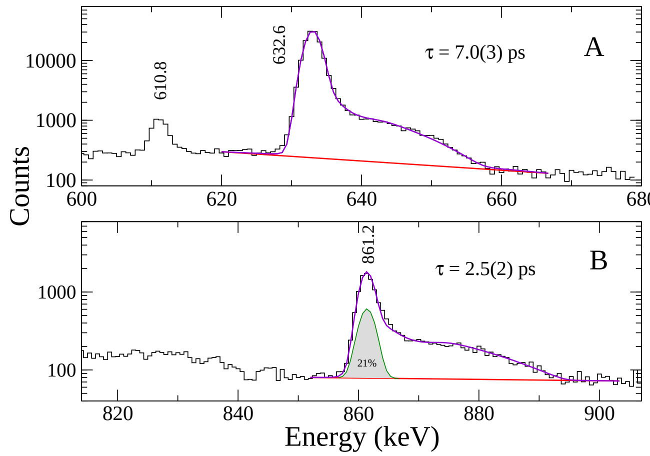

FIG. 4: Simultaneous LINESHAPE fit of the $2_1^+ \to 0_1^+$ γ line (panel A) and $4_1^+ \to 2_1^+$ γ line (panel B) in ^{106}Cd as observed in a clover segment at 68°. The shaded area represents the feeding intensity from the $4_2^+ \to 4_1^+$ γ line of 610.8 keV seen in graph A.

B. Lifetimes

On average, the cadmium ions exit the carbon foil with a velocity of 6.86% c. In Fig. 2 the γ lines of the $2_1^+ \to 0_1^+$, $4_1^+ \to 2_1^+$ and $4_3^+ \to 4_1^+$ transitions show prominent lineshapes, while the $2_2^+ \to 2_1^+$ and $3_1^- \to 2_1^+$ transitons are fully shifted and Doppler broadened. The shifted $2_2^+ \to 0_1^+$ transition is mostly hidden in the 1745.8 keV γ line of the $3_1^- \to 2_1^+$ transition. The $4_2^+ \to 4_1^+$, 610.8 keV, and $4_2^+ \to 2_1^+$, 1471.9 keV, transitions exhibit sharp γ lines indicating no decay in flight. Therefore, the mean-life of the 4_2^+ state can be estimated to be longer than 10 ps, in contrast to the NNDC report of $t_{1/2} \leq 2$ ps.

Each of the 16 HPGe crystals in the 4 clovers can be used for the DSAM lifetime analysis. The LINE-

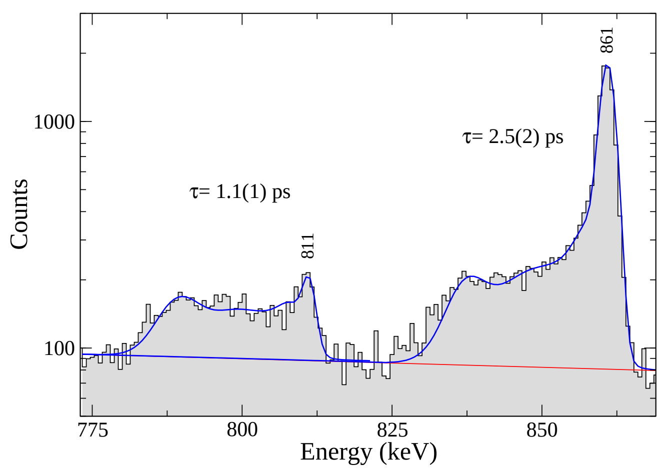

FIG. 5: LINESHAPE fit of the 811.1 keV $4_3^+ \to 4_1^+$ γ line and the 861.2 keV $4_1^+ \to 2_1^+$ γ line in ^{106}Cd as observed in a clover segment at 112°.

TABLE II: Experimental results for states in ^{106}Cd. Also included are the slopes for full clovers and the precession angles. $\Delta\theta(g=1)$ was calculated using the Rutgers parametrization [11]. The literature values of the meanlives are taken from the National Nuclear Data Center (NNDC) data base [7].

E_{Beam} (MeV)	I_i^π	E_γ (keV)	τ (ps) This work	τ (ps) NNDC [a]	$\Delta\theta(g=1)$ (mrad)	$\lvert S(60^\circ)\rvert$ (mrad^{-1})	$\Delta\theta$ (mrad)	g This work	g Others
400	2_1^+	632.6	7.0(3)	10.49(12)	98.5	1.76(3) [b]	39.14(94)	+0.398(22)	+0.393(31) [c]
410	4_1^+	861.2	2.5(2)	1.26(16)	85.7	0.66(3)	19.6(40)	+0.23(5)	
	2_2^+	1084.2	0.28(2)	0.45(7)					
		1716.5							
	4_2^+	610.8	>10	≤ 2.9					
		1471.9							
	4_3^+	811.1	1.1(1)						
	3_1^-	1745.8	0.16(1)						

[a]The NNDC publications quote half-lives
[b]$\lvert S(67^\circ)\rvert$
[c]Ref. [6]

SHAPE [12] code was used. In the first step, using a Monte Carlo simulation and Ziegler's stopping powers [13], energy-loss cascades were calculated for the reaction kinematics in the multilayer target. In the second step, the cascades relevant for each detector geometry were selected. The Doppler-broadened shapes of the γ lines were then fitted to the corresponding data sets. Sample fits are shown in Figs. 4 and 5. The results in Table II are averaged results of fits to lines in forward and backward detectors. The errors were enlarged to reflect uncertainties in feeding and the spread of the fit results in various detectors.

All the lifetimes reported in this paper have been measured for the first time by the DSAM lineshape technique and disagree with the literature values [7] determined from Coulomb-excitation cross-section B(E2) measurements. Notably, the meanlife of the 2_1^+ state is shorter by 33%, while the meanlife of the 4_1^+ state is twice the literature value. The meanlife of the 2_2^+ state is shorter by 38% and the meanlife of the 4_2^+ state is much longer. The meanlives of the 4_3^+ and the 3_1^- states have not been measured previously.

C. Magnetic moments

The Coulomb excitation of the 2_1^+ state in ^{106}Cd would be best measured below the Coulomb barrier of projectile and target nuclei. At a beam energy of 400 MeV, the adopted $g(2_1^+)$ value of +0.393(31) (Ref. [6]) was reproduced using the Rutgers parametrization [11]. In runs at 410 MeV with various beam intensities, this g factor was taken to monitor the magnetization, which is a sensitive function of the beam-spot temperature. Indeed, a strong correlation between the beam current, represented by the measured singles particle rate, and the precession rate effect of the $2_1^+ \to 0_1^+$ transition in ^{106}Cd was observed [14].

The g factor of the 4_1^+ state in ^{106}Cd was measured for the first time. This state has a short lifetime and is fed by another 4^+ state. The literature value [7] is $\tau(^{106}\mathrm{Cd}; 4_1^+) = 1.26(16)$ ps which leads to the value $g(^{106}\mathrm{Cd};4_1^+) = +0.27(6)$ quoted in Ref. [5]. A lineshape analysis of the current data yielded a new meanlife of 2.5(2) ps, and a g factor $g(^{106}\mathrm{Cd};4_1^+) = +0.23(5)$. The results are summarized in Table II.

III. DISCUSSION AND THEORY

In the present work, large-scale shell-model (LSSM) calculations were carried out for $^{106}_{48}\mathrm{Cd}_{58}$. The G-matrix interaction jj45pna was used. This interaction is included in the shell-model code *NuShellX* [15] and can be used for proton numbers below $Z = 50$ and neutron numbers above $N = 50$.

A $^{78}_{28}\mathrm{Ni}_{50}$ core was employed. The two proton valence holes below the $Z = 50$ magic number were always permitted to be anywhere in the $f_{5/2}, p_{3/2}, p_{1/2}$ and $g_{9/2}$ orbital space. Two different spaces were considered for the eight valence neutrons beyond the $N = 50$ core. Space 1 included the $g_{7/2}, d_{5/2}, d_{3/2}$ and $s_{1/2}$ neutron orbitals. Space 2 encompassed only the $g_{7/2}, d_{5/2}$ and $d_{3/2}$ orbitals. The shell-model calculations show that in both spaces the occupancies of the various orbitals are essentially the same for each of the 0_1^+, 2_1^+, and 4_1^+ states in ^{106}Cd. The proton holes are largely in the $g_{9/2}$ orbital and the neutrons are primarily in the $d_{5/2}$ and the $g_{7/2}$ orbitals.

In the $B(E2)$ calculations, two different sets of effective charges (e_p, e_n) were utilized: $(1.75e, 0.75e)$, and $(2.0e, 1.0e)$. In Table III the two corresponding calculated $B(E2)$ results are presented.

Two sets of nucleon g-factors were used in each of the two spaces for the g-factor calculations. The first set involved the *bare* g factors [$g_{lp} = 1,\ g_{sp} = 5.581,\ g_{ln} = 0,\ g_{sn} = -3.826$]. The second set included *effective* nucleon g factors [$g_{lp} = 1.1,\ g_{sp} = 4.186,\ g_{ln} = -0.1,\ g_{sn} =$

−2.870]. In each case the two calculated g-factor results are presented in Table III, first with bare and then with effective nucleon g factors.

TABLE III: Large-scale shell-model results for ^{106}Cd. The configurations used in the calculations for Space 1 and Space 2 are identified in the text. The two results quoted for the $B(E2)$'s correspond to different choices of effective charges, (e_p, e_n) as discussed in the text. Similarly, the two results for the calculated g factors correspond to choices of either bare or effective nucleon g factors, as described in the text.

	Exp't	Space 1	Space 2
$E(2_1^+)$	632.6 keV	493	685
$E(4_1^+)$	1493.8 keV	1216	1357
$B(E2; 2_1^+ \to 0_1^+)$	0.115(8) e^2b^2	0.061	0.052
		0.097	0.083
$B(E2; 4_1^+ \to 2_1^+)$	0.069(4) e^2b^2	0.083	0.055
		0.132	0.087
$g(2_1^+)$	+0.398(22)	+0.320[a]	+0.371[a]
		+0.211[b]	+0.253[b]
$g(4_1^+)$	+0.23(5)	+0.339[a]	+0.346[a]
		+0.214[b]	+0.204[b]

[a]Calculation done with bare nucleon g factors
[b]Calculation done with effective nucleon g factors

Table III shows that the calculated excitation energies $E(2_1^+)$ and $E(4_1^+)$ in Space 2 are closer to the experimental values.

Experimentally, the $g(2_1^+)$ is about twice the $g(4_1^+)$. However, the present shell-model calculations always predict values that are very close to each other.

The larger $g(2_1^+)$ value is best predicted with the bare nucleon g factors in Space 2. The smaller $g(4_1^+)$ value is well accounted for in both spaces with the effective nucleon g factors. The calculation using effective g factors always leads to predicted ^{106}Cd g-factor values that are about 70% of those predicted by the calculations using *bare* g factors.

In Ref. [6] tidal wave calculations predict for ^{106}Cd $g(2_1^+) = +0.314$ and $g(4_1^+) = +0.327$.

The corresponding calculated $B(E2)$ values, with any one set of (e_p, e_n) values, are always larger in Space 1 (which includes the $s_{1/2}$ orbital). For the $2_1^+ \to 0_1^+$ transition the results of the $B(E2)$ calculations even with $e_p = 2.0$ and $e_n = 1.0$ are only about (70 - 80)% of the experimental value. For the $B(E2; 4_1^+ \to 2_1^+)$ the calculated results agree with the experimental value best for $e_p = 1.75$, $e_n = 0.75$. Similar large effective charges were used in this region [3, 16]. Another calculation with smaller $(e_p, e_n) = (1.5,\ 0.5)$ led to $B(E2)$ results much smaller than the experimental ones and are not included in Table III.

The need for large (e_p, e_n) effective charges to explain the $B(E2)$ data indicates the presence of some collectivity in ^{106}Cd. Yet that collectivity is limited since this nucleus is only two proton holes away from the $Z = 50$ magic number.

It should be noted that simple collective models do not account for several properties of ^{106}Cd, as is detailed below.

The observed ratio of the excitation energies $E(4_1^+)/E(2_1^+)$ is 2.36; the pure vibrational model predicts 2.00 for this ratio while the pure rotational model predicts 3.33. The vibrational model predicts a degenerate $0_2^+, 2_2^+, 4_1^+$ triplet at an excitation energy of twice $E(2_1^+)$ or at 1266 keV. Experimentally, no low-lying 0_2^+ was observed in this experiment, the 4_1^+ state lies at 1493.8 keV and the 2_2^+ state is at 1716.5 keV.

The observed ratio $B(E2; 4_1^+ \to 2_1^+)/B(E2; 2_1^+ \to 0_1^+)$ = 0.599(54). This ratio is predicted to be 2.00 in the vibrational model and 1.43 in the rotational model.

Collective models predict identical values for $g(2_1^+) = g(4_1^+) = Z/A = +0.453$. Greiner [17] suggested corrections which reduce these values. The measured $g(2_1^+)$ in the present work can be explained by Greiner's approach but the $g(4_1^+)$ is still too low. A ratio of $g(2_1^+)/g(4_1^+) =$ 1.70(39) was observed here for ^{106}Cd. The highest theoretical value for $g(2_1^+)/g(4_1^+) = 1.24$, was obtained from the LSSM calculation in Space 2 with effective nucleon g factors.

IV. SUMMARY

The meanlives of the 4_3^+ and 3_1^- states in ^{106}Cd were measured for the first time. The current investigation also remeasured the meanlives of the $2_1^+, 2_2^+, 4_1^+$ and 4_2^+ levels in ^{106}Cd. In all these four cases, the new values disagree significantly with the literature values.

The current experiments also measured for the first time the $g(4_1^+)$ value in ^{106}Cd and fully reproduced the literature value of the $g(2_1^+)$. The g factor of the 4_1^+ state is about 59% that of the 2_1^+ state. This large difference cannot be explained by simple collective models, or within the framework of a tidal wave model [6]. These models predict $g(4_1^+)$ values that are very close to $g(2_1^+)$. The shell model Space 2 calculations, with effective nucleon g factors, do yield $g(2_1^+) > g(4_1^+)$ in agreement with experiment. But while these calculations are in agreement with the experimental $g(4_1^+)$ value they underpredict the $g(2_1^+)$ value. Overall, unlike some heavier Cd isotopes, ^{106}Cd is somewhat better described in the shell model based on specific single proton and neutron orbitals near the doubly-magic $N = Z = 50$ shell closure. The experimental discrepancies in the lifetimes should be resolved by future Coulomb excitation and dedicated DSAM measurements.

V. ACKNOWLEDGMENTS

The authors thank the Berkeley 88-Inch Cyclotron staff for their help in setting up the experiment and providing the cadmium beam. The target was prepared by P. Maier-Komor at the Technische Universität

Münich, Germany. The authors are grateful to L. Zamick for many discussions and suggestions about the theoretical interpretation of the g factor results. K.-H.S. acknowledges support by the Deutsche Forschungsgemeinschaft under SP190/18-1. D.A.T., Z.E.G., and F.R. acknowledge support by Colciencias under contract 110165842984 - 2015. Y.Y.S. acknowledges a Stockton University Research and Professional Development award. The work has been supported in part by the U.S. National Science Foundation and by the US Department of Energy, Office of Science, Office of Nuclear Physics under contracts No. DE-AC02-05CH11231 and DE-AC52-07NA27344 and DE-AC05-00OR22725(ORNL).

[1] P. E. Garrett, K. L. Green, and J. L. Wood, Phys. Rev. C **78**, 044307 (2008).

[2] P. E. Garrett and J. L. Wood, Journal of Physics G: Nuclear and Particle Physics **37**, 064028 (2010), URL `http://stacks.iop.org/0954-3899/37/i=6/a=064028`.

[3] A. Ekström, J. Cederkäll, D. D. DiJulio, C. Fahlander, M. Hjorth-Jensen, A. Blazhev, B. Bruyneel, P. A. Butler, T. Davinson, J. Eberth, et al., Phys. Rev. C **80**, 054302 (2009), URL `http://link.aps.org/doi/10.1103/PhysRevC.80.054302`.

[4] A. E. Stuchbery, S. K. Chamoli, and T. Kibédi, Phys. Rev. C **93**, 031302 (2016), URL `http://link.aps.org/doi/10.1103/PhysRevC.93.031302`.

[5] G. J. Kumbartzki, N. Benczer-Koller, K.-H. Speidel, D. A. Torres, J. M. Allmond, P. Fallon, I. Abramovic, L. A. Bernstein, J. E. Bevins, H. L. Crawford, et al., Phys. Rev. C **93**, 044316 (2016), URL `http://link.aps.org/doi/10.1103/PhysRevC.93.044316`.

[6] S. K. Chamoli, A. E. Stuchbery, S. Frauendorfer, J. Sun, Y. Gu, R. F. Leslie, T. P. Moore, A. Wahlke, M. C. East, T. Kibédi, et al., Phys. Rev. C **83**, 054318 (2011).

[7] D. D. Frenne and A. Negret, Nuclear Data Sheets **109**, 943 (2008), ENDSF: `http://www.nndc.bnl.gov/nndc/ensdf/`.

[8] X-Ray Instrumentation Associates: `http://www.xia.com/`.

[9] G. J. Kumbartzki, N. Benczer-Koller, S. Burcher, A. Ratkiewicz, S. L. Rice, Y. Y. Sharon, L. Zamick, K.-H. Speidel, D. A. Torres, K. Sieja, et al., Phys. Rev. C **89**, 064305 (2014).

[10] N. Benczer-Koller and G. J. Kumbartzki, J. Phys. G: Nucl. Part. Phys. **34**, R321 (2007).

[11] N. K. B. Shu, D. Melnik, J. M. Brennan, W. Semmler, and N. Benczer-Koller, Phys. Rev. C **21**, 1828 (1980).

[12] J. C. Wells and N. R. Johnson, *Computer code LINESHAPE* (1999), PD-LNL version.

[13] F. J. Ziegler, J. Biersack, and U. Littmark, *The Stopping and Range of Ions in Solids*, vol. 1 (Pergamon, Oxford, 1985).

[14] G. J. Kumbartzki, Journal of Physics: Conference Series **724**, 012027 (2016), URL `http://stacks.iop.org/1742-6596/724/i=1/a=012027`.

[15] B. A. Brown and W. D. M. Rae, Nuclear Data Sheets **120**, 115 (2014).

[16] D. A. Torres, G. J. Kumbartzki, Y. Y. Sharon, L. Zamick, B. Manning, N. Benczer-Koller, G. Gürdal, K.-H. Speidel, M. Hjorth-Jensen, P. Maier-Komor, et al., Phys. Rev. C **84**, 044327 (2011).

[17] W. Greiner, Nucl. Phys. **80**, 417 (1966).